Journal of Physics: Condensed Matter

PAPER

Corner excitations in the 2D triangle-shaped topological insulator with chiral superconductivity on the triangular lattice

To cite this article: A D Fedoseev 2020 *J. Phys.: Condens. Matter* **32** 405302

View the article online for updates and enhancements.

IOP ebooks™

Bringing together innovative digital publishing with leading authors from the global scientific community.

Start exploring the collection–download the first chapter of every title for free.

This content was downloaded from IP address 84.237.90.20 on 03/08/2020 at 14:13

IOP Publishing Journal of Physics: Condensed Matter
J. Phys.: Condens. Matter **32** (2020) 405302 (8pp) https://doi.org/10.1088/1361-648X/ab9e2f

Corner excitations in the 2D triangle-shaped topological insulator with chiral superconductivity on the triangular lattice

A D Fedoseev

Federal Research Center KSC SB RAS, Kirensky Institute of Physics, Akademgorodok 50/38, 660036 Krasnoyarsk, Russia

E-mail: fad@iph.krasn.ru

Received 15 April 2020, revised 15 June 2020
Accepted for publication 18 June 2020
Published 8 July 2020

Abstract

The 2D triangle-shaped C_3-symmetric topological insulator with the chiral superconducting coupling on the triangular lattice is investigated. While such a system cannot provide the topologically protected corner excitations, we report the presence of the nontopological corner excitations with energy value to lie in the first-order edge spectrum gap. Though these excitations are not topologically protected, they appear for a rather wide range of the parameters values and are robust against the boundary defects and weak disorder. We reveal the presence of the Majorana corner states, which appear along the line in the parameter space.

Keywords: topological insulator, edge states, chiral superconductivity

(Some figures may appear in colour only in the online journal)

1. Introduction

Recently, a novel class of condensed matter named higher-order topological insulator (HOTI) was proposed [1]. These systems are gapped both in the bulk and the first-order (conventional) edge spectrum, but contain the states located at the corner between two edges of the system and characterized by the energy in the gaps. It should be noted that the edge states arising on the domain walls between the regions with different topological numbers on the surface of the system (the second-order edge states) were investigated earlier in [2, 3]. As it was done in the case of the conventional topological insulators, the concept of the HOTI was broaden to the photonic [4, 5], acoustic [6–8] and spintronic systems [9, 10].

The special interest to the second-order edge states is caused by the existence of the Majorana corner states [11, 12] in the finite 2D higher-order topological superconductors (HOTSC). The HOTSC help to solve one of the problems of construction of the Majorana modes. One can hardly make a purely 1D system in practice, while any degree of freedom in the direction perpendicular to the main direction gives rise to the gapless band. While the zero-energy excitations still exist in such a system and separated from the bulk excitations with the gap, they are not isolated from the other edge excitations any longer. The another aspect of this problem is the changing of zero-mode edge states character from the Majorana-like state to the chiral state with changing of the stripe length and the width ratio [13, 14]. The Majorana corner states solve these problems, because they are separated with the energy gap both from the bulk and the first-order edge excitations. Additionally, they are localized precisely in the corners of the system and avoid spreading along the edges and consequently remain the Majorana-like states.

The conventional method to construct the HOTSC is to take the topological insulator and add the superconducting coupling in such way, that the first-order edge excitations become gapped with the different Dirac mass signs on the adjacent edges (e.g. [11]). In this case, the corner between the two adjacent edges becomes the domain wall and provides the gapless second-order edge state, i.e. the zero-energy corner state. While there are a lot of square-shaped HOTI and HOTSC investigations [15–19] and few studies of the corner states on the honeycomb lattice [20, 21], one can notice a lack of the investigations of the Majorana corner states on the

 © 2020 IOP Publishing Ltd Printed in the UK

triangular lattice. If we consider the triangle-shaped HOTSC on the square lattice, we can recognize two cases. The first one is connected with the situation in which the Majorana corner states appear only at two of the triangle corners [22]. The second case corresponds the situation of appearance of one corner state along with the gapless conventional edge mode [23]. The topologically protected zero-mode corner states constructed in the conventional way mentioned above appear always in pairs [24]. As a result, the only way to construct them in the odd-corner 2D systems is to break the spatial symmetries and, consequently, to point the even number of corners in which they appear.

Another way to construct the corner states was demonstrated on the example of the Kagome lattice [6, 25, 26]. The investigated system at certain values of parameters in the triangle-shaped geometry contains the decoupled sites in the corners, providing three zero-mode corner states. These states are stated to be protected by generalized chiral symmetry [6, 26] and appear at the values of parameters adiabatically connected (without closing of the bulk gap or the first-order edge spectrum gap) to this special parameter point. However, the key features of this system are the tripartite lattice and the absence of particle–hole symmetry. Consequently, it is useless to construct the HOTSC and the protected Majorana corner states. Besides the topological protection of the corner states on the Kagome lattice was argued recently [27]. Moreover, the authors of the latter investigation stated the absence of topological protection of the zero corner modes in the chiral C_3-symmetric systems.

While the topologically protected corner states contended to be forbidden in the triangle-shaped systems on the triangular lattice without breaking of the symmetry, there are two possibilities of study. The first possibility is connected with the fact that there are another manifestations of nontrivial topology besides the edge and corner states [24]. One of this manifestations is the filling anomaly, namely, the impossibility of the system to be gapped, symmetric and neutral at once. The possibility of the appearance of this anomaly in the C_3-symmetric 2D system was predicted in study [28].

The second possibility arises from the fact that the absence of the topologically protected edge states does not mean the absence of the edge states (even gapless) at all. The edge states appearing in the topologically trivial phase were detected in the 1D wire with the spin–orbit Rashba coupling, the s-wave superconducting coupling and applied magnetic field [29, 30]. The Majorana edge states were found in the trivial phase of 2D topological superconductor with the chiral superconductivity and 120° magnetic order [31, 32].

The nontopological edge states have two disadvantages. Firstly, in contrast to the topologically protected edge states there is no well known bulk-boundary correspondence for the nontopological edge states, so the conditions of their appearance must be investigated directly. Secondly, their appearance can depend on the geometry of the edge. At the same time, the gapless topologically protected edge states are not very 'protected'. They can be removed both by closing of the absolute bulk gap without changing of the topological index of the system [33] and by the little perturbation, which brakes the system symmetry and changes the topological class and, consequently, the topological index of the system without closing the bulk spectrum gap [34]. Thus, it is important to investigate the nontopological corner states in the triangle-shaped symmetric system in the absence of the topologically protected corner states.

This study is devoted to the investigation of the corner states in the triangle-shaped 2D system on the triangular lattice. Taking into account the aforesaid circumstances, this investigation seems to be important both for the theory of the second-order edge states, as well as for their possible experimental implementations. The calculations were performed for the case of the two-band topological insulator with chiral superconductivity.

2. Topological insulator with chiral superconductivity on the triangular lattice

Following the authors [11], we consider the two-band model with the Rashba spin–orbit induced hybridization and the nearest-neighbour singlet superconducting coupling in the tight-binding approximation with the Hamiltonian

$$\begin{aligned}
\mathcal{H} &= \mathcal{H}_0 + \mathcal{T} + \mathcal{H}_{\mathrm{so}} + \mathcal{H}_{\mathrm{sc}},\\
\mathcal{H}_0 &= -\mu\sum_{f\sigma} c^{\dagger}_{f\sigma}\tau_0 c_{f\sigma} + \Delta\varepsilon\sum_{f\sigma} c^{\dagger}_{f\sigma}\tau_z c_{f\sigma},\\
\mathcal{T} &= t\sum_{\langle fm\rangle\sigma} c^{\dagger}_{f\sigma}\tau_z c_{m\sigma},\\
\mathcal{H}_{\mathrm{so}} &= \mathrm{i}\lambda\sum_{\langle fm\rangle\sigma\sigma'}\left(\vec{\sigma}_{\sigma\sigma'}\times\vec{d}_{fm}\right)_z c^{\dagger}_{f\sigma}\tau_x c_{m\sigma'},\\
\mathcal{H}_{\mathrm{sc}} &= \sum_{\langle fm\rangle}\Delta_{fm}\left(a^{\dagger}_{f\uparrow}a^{\dagger}_{m\downarrow} + b^{\dagger}_{f\uparrow}b^{\dagger}_{m\downarrow}\right) + \mathrm{h.c.}\\
c^{\dagger}_{f\sigma} &= \left(a^{\dagger}_{f\sigma}, b^{\dagger}_{f\sigma}\right).
\end{aligned} \tag{1}$$

Here, the summation over f and m corresponds to the summation over the lattice sites, $\langle fm\rangle$ is summation over the nearest-neighbours, $\vec{d}_{fm}$ is the unity vector along the direction from site m to site f; μ is the chemical potential; σ_j, τ_j are the Pauli matrices in spin and two-band spaces; $a^{\dagger}_{f\sigma}, b^{\dagger}_{f\sigma}$ are the creation operator of the electron in different bands (we will refer to them as upper and lower bands correspondingly) with the difference between the on-site energy values $\Delta\varepsilon$. The spin–orbit coupling term is induced by the electric field perpendicular to the system plane, which can originate from the environment, such as the presence of substrate or heterostructure [35], or be applied and controlled directly [36, 37]. While the spin–orbit term does not preserve the electron spin projection s_z, the self-excitations of the (1) still can be classified by σ

$$\alpha_\sigma = \sum_f\left(u_{f\sigma}a_{f\sigma} + v_{f\overline{\sigma}}b_{f\overline{\sigma}} + w_{f\overline{\sigma}}a^{\dagger}_{f\overline{\sigma}} + z_{f\sigma}b^{\dagger}_{f\sigma}\right). \tag{2}$$

We consider the case of the chiral $d+\mathrm{i}d$ superconducting order parameter, which couples electrons on the

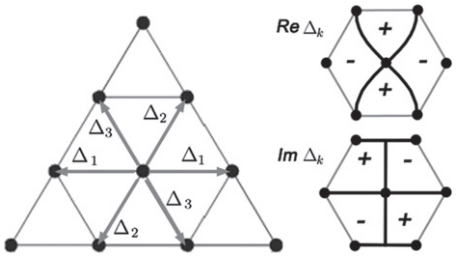

Figure 1. Chiral $d + id$ superconductivity on the triangular lattice. Left: the directions of Δ_j (3) superconducting coupling. Right: the signs of Re(Δ_k) and Im(Δ_k) [38]. Grey lines mark the edge of the Brillouin zone of the triangular lattice, the dots mark the nodal points of Δ_k (4).

nearest-neighbours and corresponds to the triangular lattice symmetry (figure 1):

$$\Delta_{fm} = \Delta_j = \Delta_1 \, e^{2\pi i(j-1)/3}, \quad j = 1, 2, 3 \tag{3}$$

The bulk excitation spectrum of the Hamiltonian (1) is given by

$$\begin{aligned} E_k &= \sqrt{|\Delta_k|^2 + \left(\mu \pm \sqrt{|t_k|^2 + |\lambda_{k\sigma}|^2}\right)^2}, \\ t_k &= \Delta\varepsilon + 2t\left(\cos\, k_x + 2\,\cos\,\frac{k_x}{2}\,\cos\,\frac{k_y\sqrt{3}}{2}\right), \\ \lambda_{k\sigma} &= 2i\lambda\sigma\left(\sin\, k_x + \sin\,\frac{k_x}{2}\,\cos\,\frac{k_y\sqrt{3}}{2}\right) \\ &\quad - 2\sqrt{3}\lambda\,\sin\,\frac{k_y\sqrt{3}}{2}\,\cos\,\frac{k_x}{2}, \\ \Delta_k &= 2\Delta_1\left(\cos\, k_x - \cos\,\frac{k_x}{2}\,\cos\,\frac{k_y\sqrt{3}}{2}\right) \\ &\quad - 2i\sqrt{3}\Delta_1\,\sin\,\frac{k_x}{2}\,\sin\,\frac{k_y\sqrt{3}}{2}. \end{aligned} \tag{4}$$

Contrary to the case studied in [11], Δ_k has the 2D representation in the case of the chiral $d + id$ superconducting coupling, and so it has the nodal points like the spin–orbital coupling instead of the nodal lines (figure 1).

In the absence of the superconducting coupling, the Hamiltonian (1) describes the chiral topological insulator. The spin Chern number [39] of the system is given by

$$\begin{aligned} C_s &= 1, \quad -6t < \Delta\varepsilon < 2t, \\ C_s &= 2, \quad 2t < \Delta\varepsilon < 3t, \end{aligned} \tag{5}$$

In the presence of the chiral superconducting coupling and the absence of the spin–orbit hybridization, the system is a topological superconductor [40, 41] with the opposite Chern numbers for the independent upper and lower bands:

$$\begin{aligned} C_+ &= 2, \quad -3t + \Delta\varepsilon < \mu < 6t + \Delta\varepsilon \\ C_- &= -2, \quad -6t - \Delta\varepsilon < \mu < 3t - \Delta\varepsilon, \end{aligned} \tag{6}$$

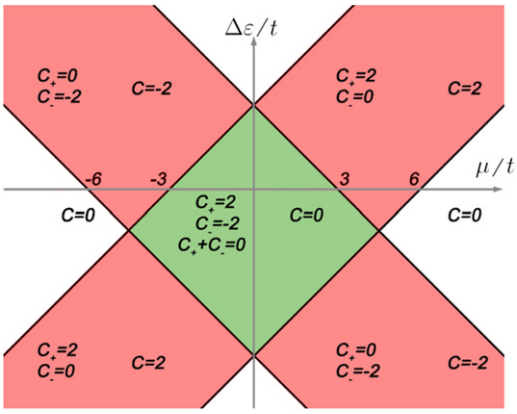

Figure 2. The topological phase diagram of the topological superconductor on the triangular lattice. In the absence of the spin–orbit coupling, the system splits into two independent subsystems for upper and lower bands providing the topologically protected edge excitations with $C_\pm = \pm 2$. The spin–orbit coupling does not change the topological properties of the trivial regions and the regions with $C_+ + C_- = \pm 2$, but since it mixes the upper and lower bands, it makes the interception region topologically trivial with $C = 0$. This opens the possibility of appearance for the corner excitations.

Note that though there are two sets of independent topologically protected excitations from the upper and lower bands at the interception of the conditions (6), the Chern number of the whole system is $C_+ + C_- = 0$. This makes this region to be sensitive to the hybridization between the bands.

The topological phase diagram of the topological insulator with chiral superconductivity on the triangular lattice remains almost the same as that without account for the spin–orbital coupling (figure 2). The regions, where in the absence of spin–orbit coupling both $C_\pm = 0$, remain trivial in the presence of the spin–orbit hybridization. The regions corresponding to one of the $C_\pm = 0$ along with $C_\mp \neq 0$ preserve the topologically protected gapless edge states with the Chern number $C = \pm 2$. Thus, the both of these cases are not interesting in the context of the corner states investigation. The main difference between the case of absence of the spin–orbital coupling and the case of its presence is that the interception region with $C = 0$ does not provide the topologically protected edge states any more, due to the spin–orbital coupling mixes the excitations from the upper and lower bands. However, this region contains the area, where the gapless edge excitations exist, and the area without them. So, this region is of the main interest of the research.

3. Nontopological corner excitations in the triangle-shaped system

We numerically calculated the self-excitations of the Hamiltonian (1) in the case of the triangle-shaped geometry in the region of main interest, mentioned in the previous section (figure 3). Depending on the different values of the model parameters, one of three cases is realized. In the first case, the system contains the gapless edge excitations, which are not topologically protected. The regions of the parameters for

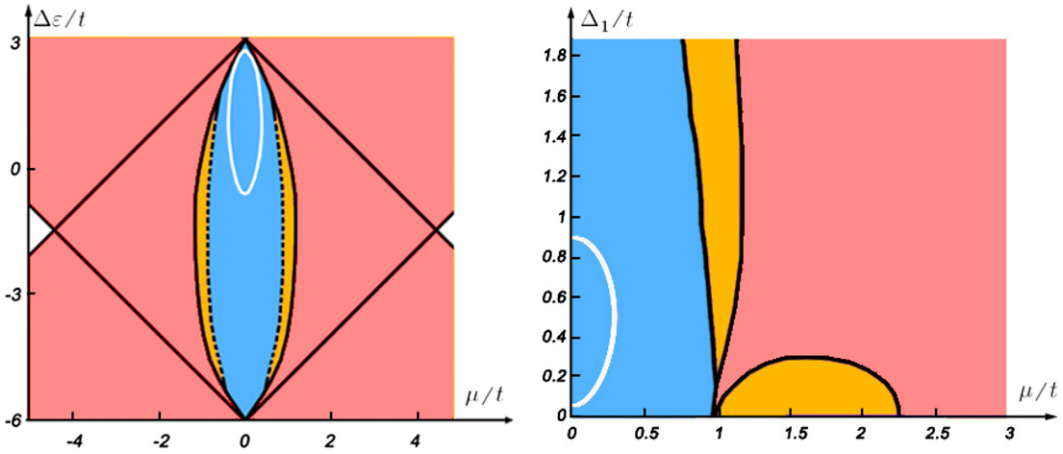

Figure 3. The parameter diagrams of the topological insulator with the chiral superconducting coupling. Left: $\Delta_1/t = 0.5$, right: $\Delta\varepsilon = 0$. The red area corresponds to the presence of the gapless first-order edge excitations at the system. The blue area shows the area of parameters for which there are corner excitations with the energies to lie inside the first-order edge spectrum gap. The orange areas marks the case, in which the conventional edge excitations are gapped, but there are no corner excitations inside the gap. White lines mark the parameters at which the Majorana corner states appear. The spin–orbit coupling parameter is $\lambda = 0.5t$.

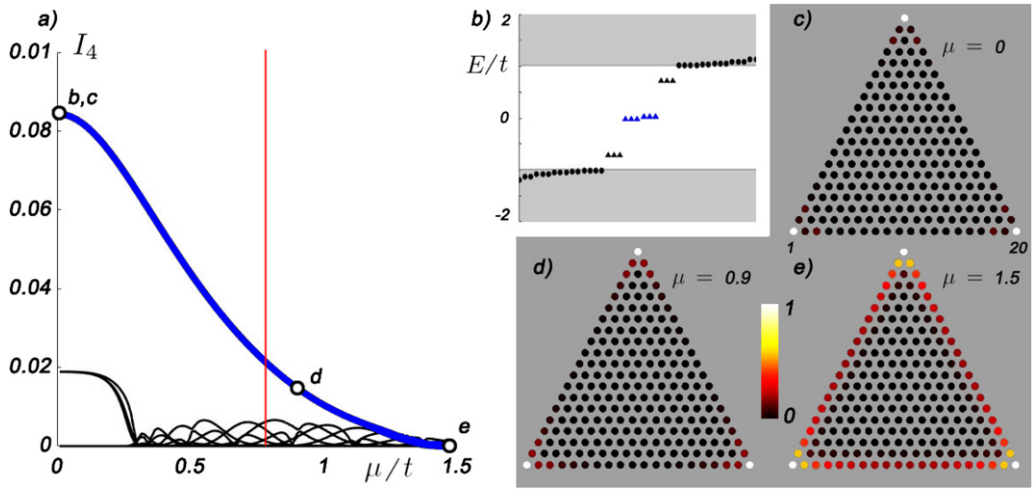

Figure 4. (a) Inverse participation ratio I_4 (7) of the self-excitations of the triangle-shaped topological insulator with chiral superconductivity. Bold blue line corresponds to the corner excitation, the vertical line marks the value of the chemical potential μ at which the corner excitation energy value crosses the bottom of the first-order edge excitations spectrum. (b) Spectrum of the system in the triangle-shaped geometry with $\mu = 0$. Dots mark the first-order excitations, triangles correspond to the corner excitations, grey regions mark the energy values, which lie inside the first-order edge excitations spectrum. (c)–(e) The spatial distribution of the normalized amplitude of the excitation for different values of μ, marked with dots in (a): at $\mu = 0$ it is the in-gap corner excitation, at $\mu = 0.9t$ it is the corner excitation with the energy value to lie outside the first-order spectrum gap, at $\mu = 1.5t$ it is the conventional edge excitation with the tendency to be localized in the corners of the limited system [46]. Here, $\Delta_1/t = 1$, $\Delta\varepsilon = 0$, $\lambda = 0.5t$.

which this case arises are connected with the regions with non-trivial topological number. In the second case, the system provides the conventional gapped edge excitations and the in-gap corner excitations. These excitations are three-order degenerated since all of three corners in the system are equivalent. In the third case, the conventional edge excitations are gapped and there are no the in-gap excitations.

In the 1D system (and the system that can be reduced to 1D), there is one-to-one correspondence between the state character and its energy. If the state energy value lies in the bulk gap, it is an edge state. If its energy value lies out of the bulk gap, it is always a bulk state. In the case of 2D systems it works only in one direction. The states with the energy value lies inside the absolute gap to be the edge states (or the corner states, if there energy is in the first-order edge spectrum gap), but they still can be edge (corner), if their energy value lies out the absolute gap. To distinguish the localized excitations from the delocalized ones, it is useful to calculate the participation ratio [42] or, more commonly, the inverse participation ratio (IPR) [43, 44], which appears to be powerful to reveal the edge states in the topological insulators [45]:

$$I_q(m) = \frac{\sum_f (A_m(f))^q}{\left(\sum_f A_m(f)\right)^q}, \tag{7}$$

where $A_m(f)$ is the amplitude of the excitation with number m at the f site and q is usually set to be $q = 2$. The IPR is a respectively large for the localized excitations ($I_q = 1$, if the excitation is localized precisely at one site) and tends to be $I_q = 1/V^{q-1}$ for the extended excitations in the system with V sites.

We used the quantity $q = 4$ instead of common $q = 2$, because the last one was not enough to distinguish the corner states from the first-order edge states clearly according to the limited size of the system. The I_4 dependence on μ is demonstrated in the figure 4. One can see that the self-excitation has the maximum I_4 and in-gap energy at $\mu = 0$ and is localized well at the corners of the triangle. This self-excitation remains a second-order excitation even after its energy value crosses the bottom of the first-order edge spectrum. The small I_4 peaks arise owing to the effect of the presence of corners on the first-order edge excitations. This effect consists in the tendency of the first-order edge excitations with the energy value lies deep inside the bulk gap to localize in the corners [46]. They can be recognized at the change of the system size. Indeed, as far as they are still the edge states, the IPR is decreased at the increase in the system size, while the IPR of the corner excitation remains unchanged.

Besides the corner excitations with nonzero energy, we reveal the presence of the Majorana corner states in the system under consideration at the certain parameters (white line in the figure 3). Contrary to the parameter lines in [30, 47, 48], the line of parameters for which Majorana states appear in our case remains independent on the system size (for not very small systems) and, consequently, is not a size effect. The presence of the Majorana corner states in the system is robust against the disorder or defects, but the parameters at which they appear are sensitive to the disorder and defects in the corners of the system (see appendix A for details).

Thus, we demonstrate that even in the absence of the topologically protected corner excitations with the energies localized precisely at zero, the studied system demonstrates the nontopological corner excitations for rather wide area of parameters, as well as the Majorana corner states. Nevertheless, these corner excitations are not topologically protected, they demonstrate robustness under boundary defects and disorder.

4. Conclusion

The triangle-shaped two-band topological insulator with the Rashba spin–orbital coupling and chiral superconducting order parameter is investigated. It is shown that though the system cannot provide the topologically protected corner excitations, it still can provide the corner excitations of nontopological character with energy value lies in the first-order edge spectrum gap. It was revealed that despite the fact these excitations are not protected, they appear at rather wide ranges of parameters and are localized well in the corners of the system. As their energies are not pinned at zero value, they are changed with changing of the parameters. The revealed excitations preserve second-order character even after its energy value crosses the bottom of the first-order edge excitations spectrum. The parameters, for which the corner excitations arise, correspond to the phase of the two-band topological superconductor without the inter-band hybridization providing the topologically protected conventional edge excitations with the zero full Chern number. The revealed corner excitations demonstrate robustness against the boundary defects and weak disorder.

Additionally, it is shown that even in the absence of the topologically protected Majorana modes appearing at the domain walls between the edges, the triangle-shaped symmetric system still can provide well localized Majorana corner states at the certain parameters, which form the line in the parameter space.

Acknowledgments

The author thanks D M Dzebisashvili, M S Shustin, V A Mitskan and M M Korovushkin for the fruitful discussions and valuable remarks. The reported study was funded by the Russian Foundation for Basic Research (Projects Nos. 19-02-00348, 19-42-240011) and the Council of the President of the Russian Federation for Support of Young Scientists and Leading Scientific Schools (Project MK-1641.2020.2).

Appendix A. Robustness of the corner excitations in the 2D triangle-shaped topological insulator with chiral superconductivity on the triangular lattice

The topologically protected edge excitations are robust against the defects and perturbations, which preserves the symmetry protecting the edge excitations and remains the gap open. As far as the corner excitations revealed in the triangle-shaped topological insulator with chiral superconductivity on the triangular lattice are not topological, we have to investigate their robustness under perturbations.

A.1. Boundary defects

Firstly, we investigate the effect of the boundary defect, located far from the corners, on the self-excitations of the system (figures A1(a)–(c)). As can be expected, the corner excitations remains almost insensitive to removal or addition of the site on the boundary. At the same time there appear several excitations with the in-gap energy, localized at the defect.

Secondly, we examine the influence of the defect consisting in removal (figures A1(d)–(f)) or attaching (figures A1(g)–(i)) of sites in the corner of triangle on the corner excitations of the investigated system. Just as in the previous case, the excitations in the corners far away from the defect remains insensitive. The corner excitations in the defected corner remains, but slightly change their shape according to the shape of defect. Additionally, the number of excitations corresponding to the defected corner increases.

In both cases the revealed corner excitations demonstrate their robustness against small boundary defects, and only slightly change according to the defect shape, if the defect locates in the corner or near it. If the defect is large

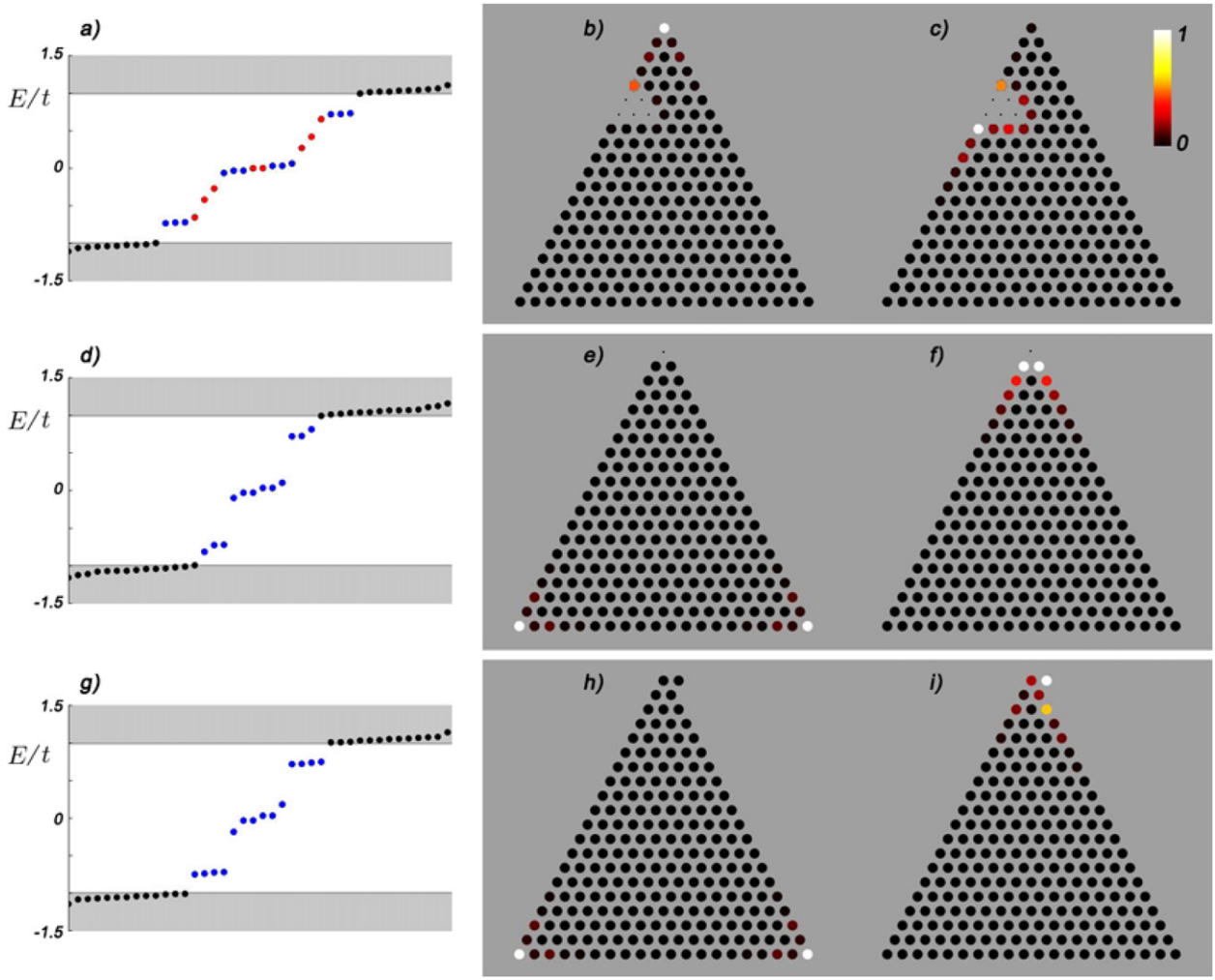

Figure A1. Spectrum (a), (d) and (g) and normalized amplitude (b) and (c), (e) and (f) and (h) and (i) of the excitations in the case of triangle-shaped system with boundary defect, located far from the corners (a)–(c), and with boundary defect, located in the corner and consisted in removing (d)–(f) or attaching (g)–(i) a site. The blue dots on the panels (a), (d) and (g) corresponds to the corner excitations (b), (e) and (f) and (h) and (i), while red dots mark the excitations located at the defect (c). Here, $\Delta_1/t = 1$, $\Delta\varepsilon = 0$, $\lambda = 0.5t$, $\mu = 0$.

enough, the excitations, located at the corners of the defect, appear.

The parameter lines, at which zero modes appear, are also robust under defects, which are located far from the corners. At the same time there can appear new parameter lines, at which zero modes located at the defect realize. In the case of the defect, located at the corner, the zero energy excitation corresponding to this corner remains but appears at another parameter values.

A.2. Disorder

To examine the robustness of the revealed corner excitations against the disorder following [49] we use the additional term to the Hamiltonian (1):

$$\mathcal{H}_{\text{do}} = \sum_{f\sigma} V_f c^{\dagger}_{f\sigma} \tau_0 c_{f\sigma}, \tag{A.1}$$

where V_f is a random on-site disorder potential with uniform distribution for $|V_f| < V$.

Series of numerical calculations demonstrates that small disorder remove the degeneracy of the corner excitations, but remains their form almost unchanged (figures A2(a) and (b)). Moreover, rather large disorder of $V = 1.5t$, which force the first-order excitations to demonstrate the tendency to Anderson localization, remains almost unchanged even the corner excitations with energy outside of the conventional edge gap (figures A2(c) and (d)).

Just as it was in the case of the defect, located in the corner, the zero energy excitations remain in the case of disorder, but the chemical potential μ, at which they appear, can significantly change and become different for the excitations in the different corners. The shift for the zero-mode parameter line is obviously connected with the disorder potential values in the corner (especially on the corner site), and is vanishing, if this potential take the zero value at the corner site. Thus one have to prevent the disorder and defects at the corners of the triangle to find the zero-modes at the lines of parameters, revealed in the main text. At the same time, the parameters, at which the non-zero corner excita-

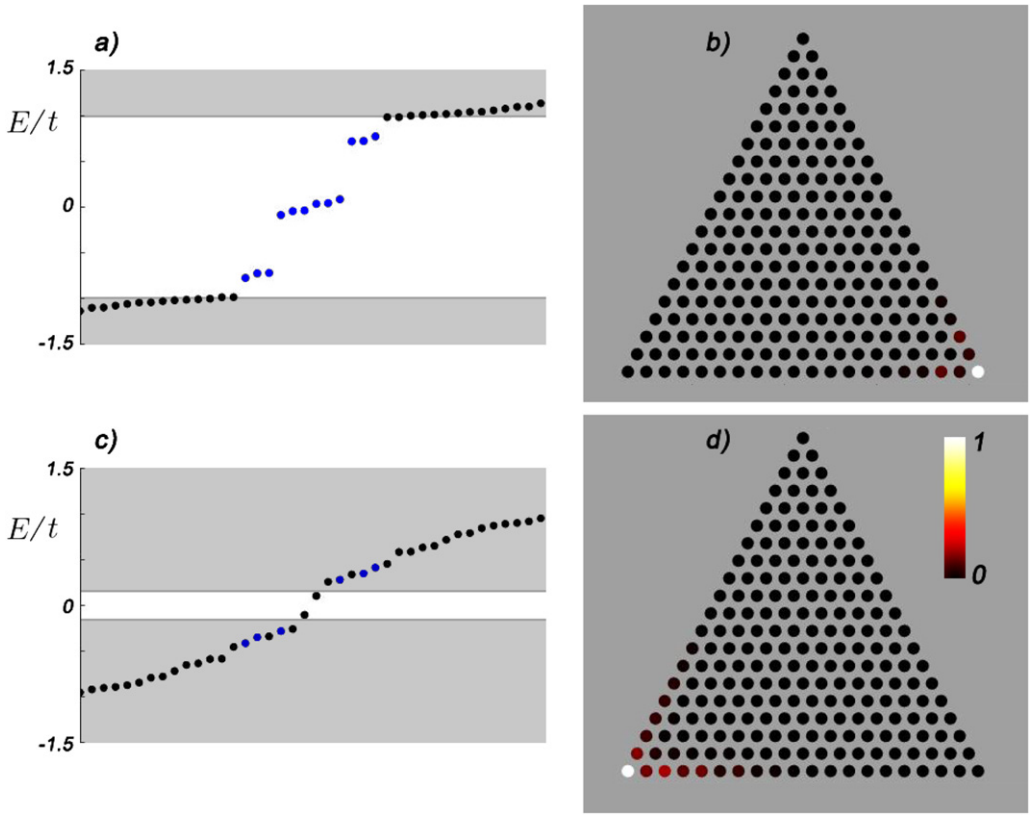

Figure A2. Typical spectrum and normalized amplitude of the corner excitations for the case of small disorder $V = 0.5t$ and $\mu = 0$ (a) and (b) and for the case of large value of disorder $V = 1.5t$ and $\mu = 0.9t$ (c) and (d). Blue circles in the panels (a) and (b) marks well localized corner excitations, grey regions mark the energy values, which lie inside the first-order edge excitations spectrum without disorder. Here, $\Delta_1/t = 1$, $\Delta\varepsilon = 0$, $\lambda = 0.5t$.

tions appear inside the gap, slightly depend on the defects or disorder.

ORCID iDs

A D Fedoseev https://orcid.org/0000-0002-3073-2101

References

[1] Benalcazar W A, Bernevig B A and Hughes T L 2017 *Science* **357** 61
[2] Zhang F, Kane C L and Mele E J 2013 *Phys. Rev. Lett.* **110** 046404
[3] Volovik G E 2010 *J. Exp. Theor. Phys. Lett.* **91** 201
[4] Hassan A E, Kunst F K, Moritz A, Andler G, Bergholtz E J and Bourennane M 2019 *Nat. Photon.* **13** 697
[5] Chen X-D, Deng W-M, Shi F-L, Zhao F-L, Chen M and Dong J-W 2019 *Phys. Rev. Lett.* **122** 233902
[6] Ni X, Weiner M, Alu A and Khanikaev B 2019 *Nat. Mater.* **18** 113
[7] Xue H, Yang Y, Liu G, Gao F, Chong Y and Zhang B 2019 *Phys. Rev. Lett.* **122** 244301
[8] He C, Yu S-Y, Wang H, Ge H, Ruan J, Zhang H, Lu M-H and Chen Y-F 2019 *Phys. Rev. Lett.* **123** 195503
[9] Li Z-X, Cao Y, Wang X R and Yang P 2019 arXiv:1910.03956
[10] Li Z-X, Cao Y, Wang X R and Yang P 2020 *Phys. Rev.* B **101** 184404
[11] Wang Q, Liu C-C, Lu Y-M and Zhang F 2018 *Phys. Rev. Lett.* **121** 186801
[12] Zhu X 2018 *Phys. Rev.* B **97** 205134
[13] Potter A C and Lee P A 2010 *Phys. Rev. Lett.* **105** 227003
[14] Sedlmayr N, Aguiar-Hualde J M and Bena C 2016 *Phys. Rev.* B **93** 155425
[15] Ghorashi S A A, Hu X, Hughes T L and Rossi E 2019 *Phys. Rev.* B **100** 020509
[16] Yoshida A, Otaki Y, Otaki R and Fukui T 2019 *Phys. Rev.* B **100** 125125
[17] Zou J, He Z and Xu G 2019 *Phys. Rev.* B **100** 235137
[18] Pozo O, Repellin C and Grushin A G 2019 *Phys. Rev. Lett.* **123** 247401
[19] Roy B 2019 *Phys. Rev. Res.* **1** 032048
[20] Mizoguchi T, Araki H and Hatsugai Y 2019 *J. Phys. Soc. Japan* **88** 104703
[21] Ren Y, Qiao Z and Niu Q 2020 *Phys. Rev. Lett.* **124** 166804
[22] Yan Z, Song F and Wang Z 2018 *Phys. Rev. Lett.* **121** 096803
[23] Wu Y-J, Hou J, Luo X, Li Y and Znag C 2020 *Phys. Rev. Lett.* **124** 227001
[24] Khalaf E, Benalcazar W A, Hughes T L and Queiroz R 2019 arXiv:1908.00011
[25] Ezawa M 2018 *Phys. Rev. Lett.* **120** 026801
[26] Kempkes S N, Slot M R, van den Broeke J J, Capoid P, Benalcazar W A, Vanmaekelbergh D, Cercioux D, Swart I and Smith C M 2019 *Nat. Mater.* **18** 1292
[27] Miert G and Ortix C 2020 arXiv:2005.00560
[28] Benalcazar W A, Li T and Hughes T L 2019 *Phys. Rev.* B **99** 245151
[29] Serina M, Loss D and Klinovaja J 2018 *Phys. Rev.* B **98** 035419
[30] Fedoseev A D 2019 *J. Exp. Theor. Phys.* **128** 125
[31] Val'kov V V, Zlotnikov A O, Fedoseev A D and Shustin M S 2017 *J. Magn. Magn. Mater.* **440** 37

[32] Val'kov V V, Zlotnikov A O and Shustin M S 2018 *J. Magn. Magn. Mater.* **459** 112
[33] Malki M and Uhrig G S 2019 *Europhys. Lett.* **127** 27001
[34] Ezawa M, Tanaka Y and Nagaosa N 2013 *Sci. Rep.* **3** 2790
[35] Bychkov Yu A and Rashba E I 1984 *J. Phys. C: Solid State Phys.* **17** 6039
[36] Nitta J, Akazaki T and Takayanagi H 1997 *Phys. Rev. Lett.* **78** 1335
[37] Schapers T, Knobbe J and Guzenko V A 2004 *Phys. Rev.* B **69** 235323
[38] Black-Schaffer A M and Honerkamp C 2014 *J. Phys.: Condens. Matter* **26** 423201
[39] Ezawa M 2012 *Eur. Phys. J.* B **85** 363
[40] Senthil T, Marston J B and Fisher M P A 1999 *Phys. Rev.* B **60** 4245
[41] Chern T 2016 *AIP Adv.* **6** 085211
[42] Bell R J and Dean P 1970 *Discuss. Faraday Soc.* **50** 55
[43] Thouless D J 1974 *Phys. Rep.* **13** 93
[44] Murphy N C, Wortis R and Atkinson W A 2011 *Phys. Rev.* B **83** 184206
[45] Calixto M and Romera E 2015 *J. Stat. Mech.* P06029
[46] Fedossev A D 2020 *J. Phys.: Condens. Matter* **32** 215301
[47] Val'kov V V, Mitskan V A and Shustin M S 2017 *J. Exp. Theor. Phys. Lett.* **106** 798
[48] Val'kov V V, Mitskan V A and Shustin M S 2019 *J. Exp. Theor. Phys.* **129** 426
[49] Kobayashi K, Ohtuski T and Imura K-I 2013 *Phys. Rev. Lett.* **110** 236803